Received 8 March 2024; revised 14 May 2024 and 13 September 2024; accepted 2 October 2024. Date of publication 7 October 2024; date of current version 23 December 2024. The review of this article was arranged by Editor B. Iñiguez.

Digital Object Identifier 10.1109/JEDS.2024.3475513

Utilization of Graphite Nanoparticles as a Hybrid Hole Transport Layer in Non-Fullerene Organic Solar Cells

MAGALY RAMÍREZ-COMO[1] (Member, IEEE), MONICA M. VALDEZ-MATA[1], ANGEL SACRAMENTO[2] (Member, IEEE), JOSÉ L. CASAS-ESPÍNOLA[3], LUIS RESÉNDIZ[1] (Member, IEEE), AND LLUIS F. MARSAL[4] (Senior Member, IEEE)

1 Sección de Estudios de Posgrado e Investigación, UPIITA, Instituto Politécnico Nacional, Mexico City 07340, Mexico
2 Sección de Electrónica del Estado Sólido, Departamento de Ingeniería Eléctrica, CINVESTAV-IPN, Mexico City 07360, Mexico
3 Escuela Superior de Física y Matemáticas, Instituto Politécnico Nacional, Mexico City 07738, Mexico
4 Departament d'Enginyeria Electronica Electrica i Automatica, Rovira i Virgili University, 43007 Tarragona, Spain

CORRESPONDING AUTHORS: M. RAMÍREZ-COMO AND L. F. MARSAL (e-mail: magaly.ramirez@cinvestav.mx; lluis.marsal@urv.cat)

This work was supported in part by the Spanish Ministerio de Ciencia e Innovación (MICINN) under Grant PDI2021-128342OB-I00; in part by the Secretaria d'Universitats i Recerca del Departament de Recerca i Universitats de la Generalitat de Catalunya under Grant AGAUR-2021 SGR 00739 GRC; in part by the Catalan Institution for Research and Advanced Studies (ICREA) under the ICREA Academia Award 2021; in part by the Secretaría de Investigación y Posgrado del Instituto Politécnico Nacional under Grant 20242346 and Grant 20232319; and in part by the Consejo Nacional de Humanidades, Ciencias y Tecnologías (CONAHCYT) under Grant BPPA-20220624083033039-2364083 awarded to CVU 704226 and Grant CVU 1022110.

This article has supplementary downloadable material available at https://doi.org/10.1109/JEDS.2024.3475513, provided by the authors.

ABSTRACT This study investigates the impact of incorporating graphite nanoparticles (GNPs) into poly(3,4-ethylenedioxythiophene):poly(styrenesulfonate) (PEDOT:PSS) as hybrid hole transport layer (HTL) in non-fullerene organic solar cells (NF-OSCs) based on PBDB-T-2F:BTP-4CL. The concentration of GNPs in the PEDOT:PSS layer was varied to investigate their impact on the overall device behavior. The PCE initially increased with the GNPs concentration up to 5% v/v, reaching a maximum enhancement of 6.43%, which was attributed to the increased J_{SC}. Current-voltage measurements and Mott-Schottky analysis through capacitance-voltage characteristics were conducted to evaluate the behavior of the charge recombination and built-in potential due to the concentration variation of the GNPs into PEDOT:PSS. This study illustrates the potential of GNPs to improve OSC performance through enhanced light absorption, reduced recombination losses, and improved charge carrier transport, indicating promising prospects for GNPs on interface layers in OSCs.

INDEX TERMS Carbon dots, charge carrier recombination mechanism, graphite carbon nanoparticles, hybrid hole transport layer, non-fullerene solar cells, PEDOT:PSS dopants.

I. INTRODUCTION

Research in organic solar cells aims to develop new materials to improve the efficiency. The inception of emerging non-fullerene acceptors (NFAs) by replacing the fullerene counterpart in organic solar cells (OSCs) has pushed the bulk-heterojunction (BHJ)-based photovoltaics to achieve efficiencies approaching 19% [1], [2], [3], [4], [5]. The BTP-4CL (Y7) NFA molecule has improved power conversion efficiencies (PCEs) by minimizing the trade-off between voltage loss and charge generation in NF-OSCs [6], [7]. Furthermore, they have strong absorption in the near-infrared region with donor polymers and the ability to tune their energy levels [8], [9]. These properties improve the charge-carrier mobility and light absorption of the corresponding devices.

To further improve the performance of OSCs, a central element is the hole-transport layer (HTL), which facilitates the movement of charge carriers within the device. Poly-(3,4ethylenedioxythiophene): poly(styrenesulfonate) (PEDOT:PSS) is a popular choice for HTL in OSCs owing to its remarkable conductivity, excellent transparency, and suitable work function [10], [11]. Moreover, additional modification of PEDOT:PSS has been conducted utilizing

nanoparticles (NPs) to increase the conductivity and stability of PEDOT:PSS, thereby optimizing its performance as an HTL. NPs synthesized through various methods exhibit an augmented light field and localized surface plasmon resonance, thereby enhancing the absorption of the active layer [10]. NPs materials such as graphene oxide, Au, WS_2, WSe_2, and In_2Se_3 have emerged as effective modifiers or alternatives for HTL enhancement [12], [13], [14], [15], [16]. These materials exhibit high conductivities, superior carrier mobilities, and tunable energy levels. Wang et al. demonstrated an enhanced PCE of 15.89% based on PBDB-T-2F:Y6 NF-OSCs by incorporating In_2Se_3 nanosheets as HTL additives, which was attributed to improved PEDOT:PSS conductivity, hole mobility, and optimized HTL surface morphology [13]. Hao et al. observed enhanced performance by incorporating Au NPs of various shapes (rods, bones, cubes, and others) into PEDOT:PSS, achieving a PCE of 9.26% in OSCs [16]. Similarly, Lin et al. introduced WS_2 into PEDOT:PSS, enhancing the charge extraction of the HTL and achieving a remarkable increase in the maximum PCE of 17.0% in OSCs based on PBDB-T-2F:Y6:$PC_{71}BM$ ternary structures [12].

Graphite nanoparticles (GNPs) have emerged as compelling candidates because of their easy synthesis, good dispersion, and combination of electrical and mechanical properties [17], [18]. GNPs, owing to their high conductivity, offer promising avenues for enhancing charge transport and improving interfacial interactions within OSCs. These materials boast high conductivity, superior carrier mobilities, and tunable energy levels.

In this paper, we report the use of graphite nanoparticles as a hybrid hole-transport layer in non-fullerene organic solar cells (NF-OSCs). The active blend used was PBDB-T-2F (PM6) as the donor material and BTP-4CL (Y7) as the acceptor material. The fabricated NF-OSCs had the following structure: ITO/HTL/PBDB-T-2F:BTP-4CL/PDINO/Ag. Comparative studies were performed to investigate the effect of these graphite nanoparticles on the overall performance of the fabricated solar cells.

II. EXPERIMENTAL SECTION

A. MATERIALS

An indium tin oxide (ITO) patterned glass substrate (resistivity of 10 Ω/sq) was used as a transparent conducting oxide and was purchased from Xin Yan Technology Ltd. The BTP-4CL non-fullerene acceptor, PBDB-T-2F polymer donor, and PDINO materials were acquired from One-Material, Inc. High-purity silver (99.99%) wire was obtained from Testbourne Ltd. PEDOT:PSS (Clevios P VP.Al 4083) was obtained from Heraeus.

B. PREPARATION OF GRAPHITE NANOPARTICLES (GNPS)

Graphite nanoparticles (GNPs) were synthesized via a hydrothermal route. First, 1 g of citric acid ($C_6H_8O_7$) and 2 g of urea (NH_2CONH_2) as carbon sources were diluted in 40 ml of deionized water. The solution was heated in an autoclave at 200 °C for 5 h. The solution was then filtered through a 3.5 kD dialysis membrane. Finally, a suspension of GNPs was synthesized and directly used in the precursor solution of hole transport layer (HTL).

C. DEVICE FABRICATION

The fabricated NF-OSC was based on the ITO/HTL/PBDB-T-2 F:BTP-4CL/PDINO/Ag structure. ITO glass substrates were initially cleaned in deionized water and a soap solution, followed by ultrasonic bathing in high-purity solvents of acetone, methanol, and isopropanol sequentially for 10 min each. Subsequently, the cleaned substrates were oven-dried at 100 °C for 10 min. Before depositing the first layer, the substrates were UV a UV-ozone treatment for 30 min. The first layer, PEDOT:PSS, served as the hole transport layer and was filtered through a 0.2 μm filter. Subsequently, PEDOT:PSS without and with different concentrations of GNPs (5, 10, and 20% v/v) was spin-coated at 4000 rpm for 40 s on top of the glass/ITO substrate and annealed for 15 min at 150 °C in air. The PEDOT:PSS-coated ITO substrates were placed in a nitrogen-filled glove box for active-layer deposition. The PBDB-T-2F:BTP-4CL solution was prepared as detailed in [2], [3], [19], [20]. The electron transport layer, PDINO (1.5 mg/ml in methanol), was subsequently deposited by spin coating at 3000 rpm for 30 s. Finally, the substrates were transferred into an evaporation chamber inside a glove box, where Ag was thermally evaporated through a shadow mask deposited under high vacuum conditions ($\leq 1\times10^{-6}$ mbar) to form photovoltaic devices with an area of 0.09 cm^2.

D. CHARACTERIZATION AND MEASUREMENT

The structure of the graphite nanoparticles was observed using high-resolution transmission electron microscopy (HR-TEM; JEOL JEM 2100). The interplanar distances were measured using the Digital Micrograph program, and the database used to verify the information was obtained from PANalytical. UV–Vis absorption spectra were obtained using a SHIMADZU UV 1800 equipment. Photoluminescence (PL) spectra were obtained at a power of 40 mW using a COHERENT Verdi model V-5 solid-state laser, He-Cd laser, and Ar+ laser at excitation wavelengths of 532, 325, and 488 nm, respectively.

The conductivities of the HTLs were probed by current density – voltage (J–V) characteristics using a Keithley 2400 source-measure unit.

The J–V characteristics of the solar cells were measured under the AM1.5 spectrum using a solar simulator (Abet Technologies model 11 000 class type A, Xenon arc). The measurements were performed at room temperature using a Keithley 2400 source-measure unit. To calibrate the intensity of the solar simulator a Fraunhofer certified photovoltaic cell was utilized to obtain an irradiance of 100 mW/cm^2. A series of optical density filters was employed to achieve different

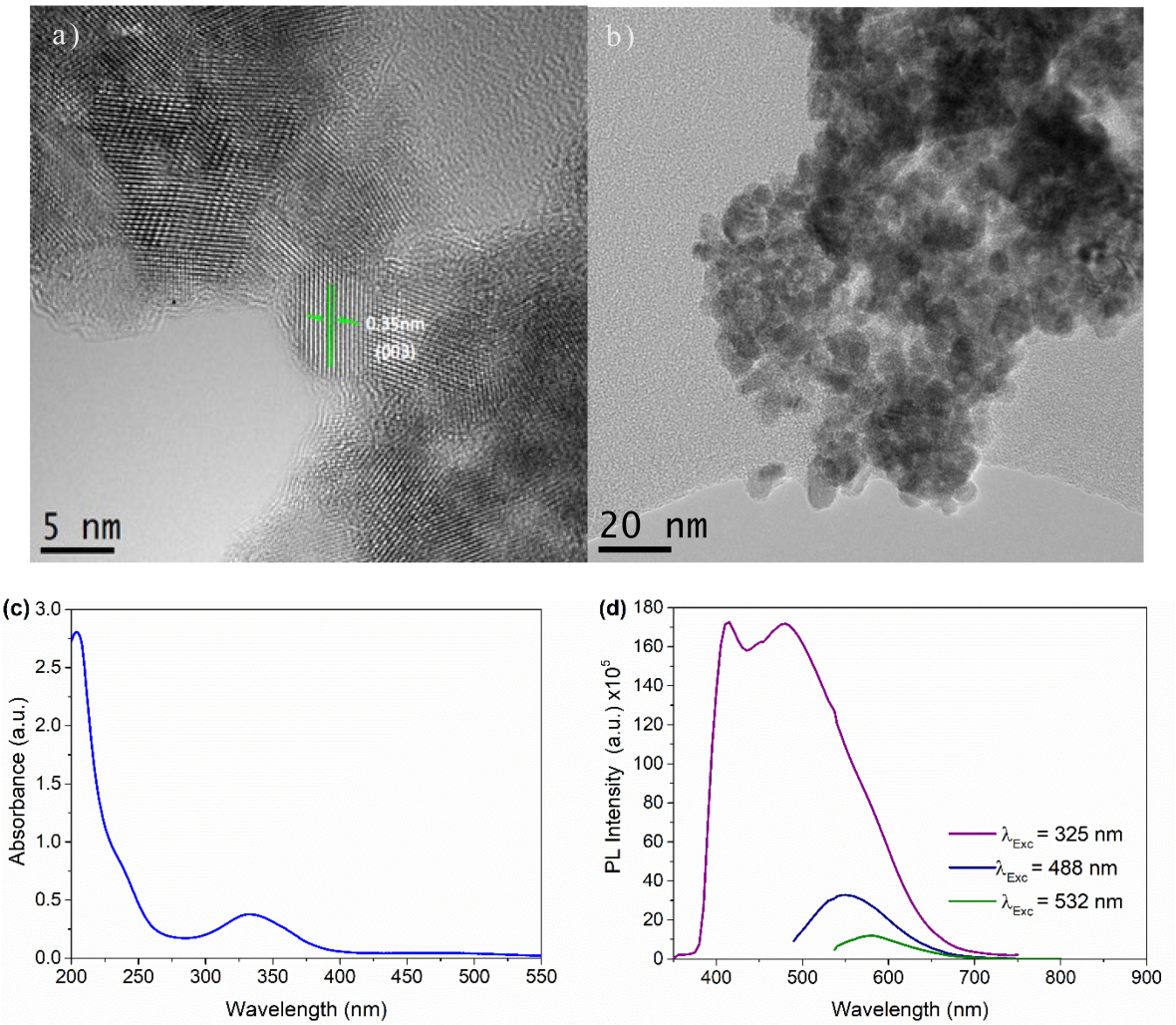

FIGURE 1. **HR-TEM images of GNPs (a) interplanar distance, and (b) particle population; (c) UV-Vis absorbance spectrum; (d) PL emission spectra at excitation wavelengths of 325 nm, 488 nm, and 532 nm.**

light intensities under one-sun illumination. The external quantum efficiency (EQE) spectra of the solar cells were measured using Lasing IPCE-DC model equipment, and the system was calibrated using a photodiode in the device under the test position. The optical transmittance was measured at room temperature from 300 to 1000 nm using a Perkin Elmer Lambda 950 UV/VIS/NIR recording spectrophotometer.

III. RESULTS AND DISCUSSION

In this study, we analyzed the incorporation of graphite nanoparticles into PEDOT:PSS as a hybrid HTL in the NF-OSCs structure based on PBDB-T-2F:BTP-4CL. Before their application in organic solar cells, we characterized the structure of the GNPs using HR-TEM. Fig. 1 shows the HR-TEM images of GNPs, it can be observed an interplanar distance of $\sim$ 0.35 nm (Fig. 1 (a)) that corresponding to (003) plane of graphite hexagonal structure. Besides, the size distribution of the GNPs ranges from 2.9 to 6.4 nm, indicate average sizes of 5.05 nm (Fig. 1 (b)).

To explore the optical properties of the GNPs, both UV-Vis absorption spectra and the PL spectra of the GNPs were measured, as shown in Fig. 1 (c)–(d). The UV-V is absorbance spectrum (Fig. 1 (c)) shows a peak at $\sim$ 335 nm, attributed to the n-π* transition of the C=C bond of the GNPs [21]. Photoluminescence spectroscopy, shows in Fig. 1 (d), indicates that as the excitation wavelength increases, the emission wavelength shifts towards red, which is a phenomenon characteristic of GNPs [22]. The Raman and FTIR spectra of the GNPs are shown in the Supporting Information.

To evaluate the effect of GNPs on the electrical properties of the hybrid HTL, the conductivity of the hybrid films with different concentrations of GNPs (5, 10, and 20% v/v) into PEDOT:PSS was investigated. Devices with the ITO/PEDOT:PSS+GNPs/Ag structure were fabricated (shown in the inset of Fig. 2 (a)), and the corresponding I-V characteristics of the devices were measured, as shown in Fig. 2 (a). It can be observed that the slope of the I-V curves initially increased and then decreased with an increasing amount of GNPs into PEDOT:PSS. The pristine PEDOT:PSS films showed a conductivity of 6.80×10^{-6}

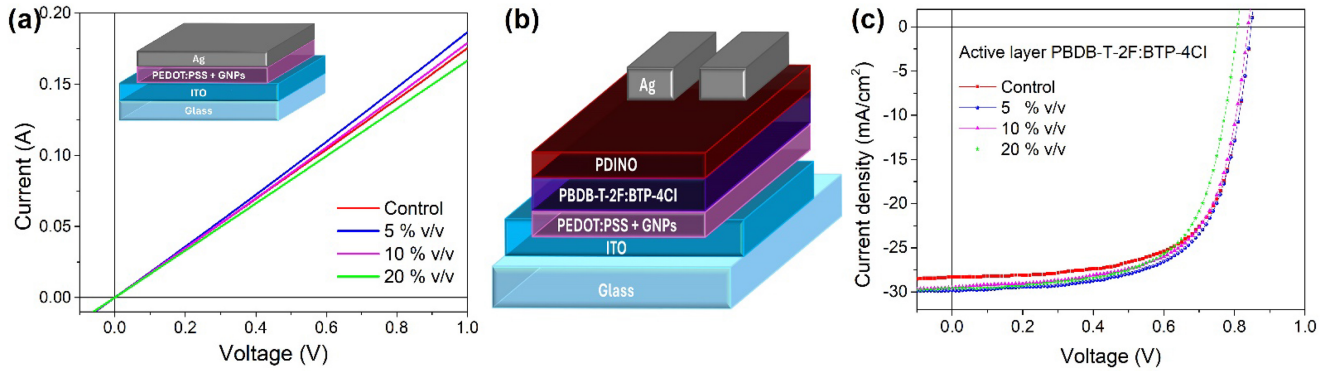

FIGURE 2. **(a) Variation in the electrical conductivity of PEDOT:PSS incorporating different concentrations of GNPs; (b) device structure of OSCs based on PBDB-T-2F:BTP-4CL with PEDOT:PSS+GNP hybrid HTL; (c) *J-V* curves of the best NF-OSCs incorporated with different concentrations of GNPs into PEDOT:PSS.**

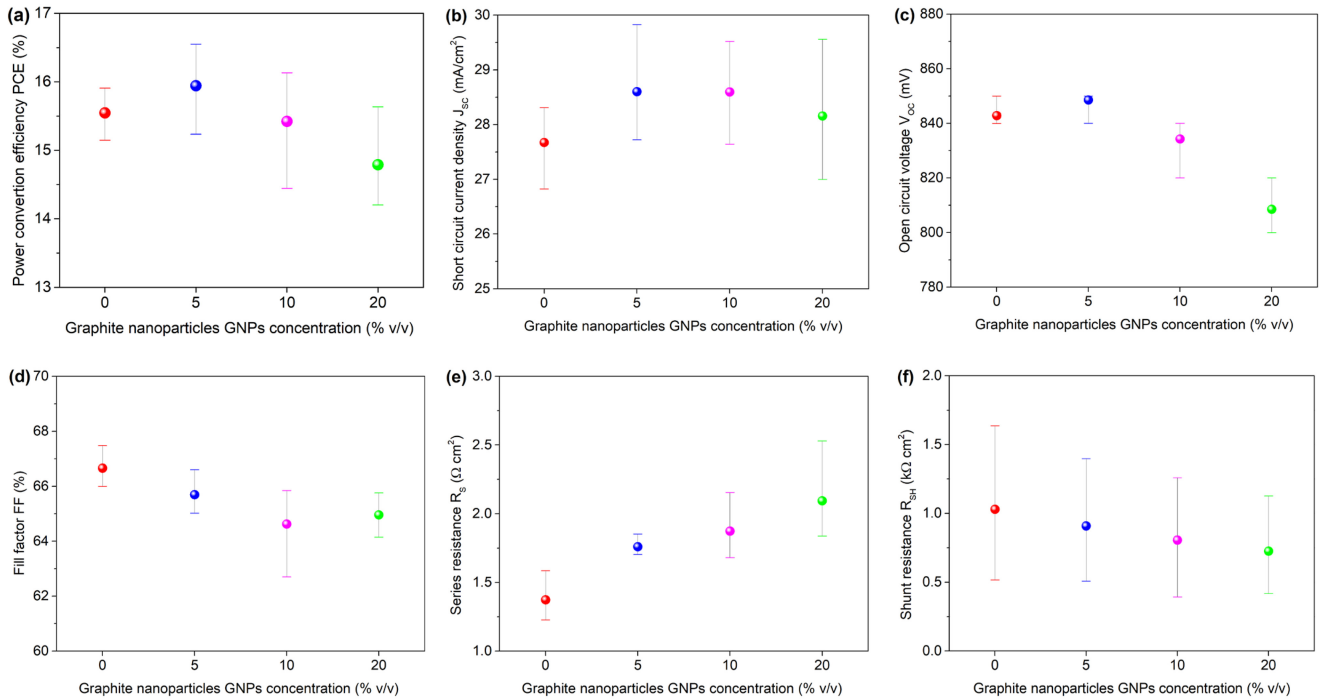

FIGURE 3. **The graphite nanoparticles concentration dependent performance parameters for NF-OSCs based on PBDB-T-2F:BTP-4CL: (a) PCE; (b) J_{SC}; (c) V_{OC}; (d) FF; (e) R_S and (f) R_{SH}. The error bars correspond to the maximum and minimum values obtained under the respective conditions.**

S/cm. After GNPs doping, the hybrid HTL showed enhanced conductivities of 7.25×10^{-6} S/cm, and 6.95×10^{-6} S/cm, when the concentration of GNPs reached 5, and 10% v/v, respectively. After that, when the amount of GNPs was further increased, the conductivity value decreases to 6.95×10^{-6} S/cm.

To further explore the potential of GNPs into PEDOT:PSS as a hybrid HTL, NF-OSCs were fabricated with a device structure, as shown in Fig. 2 (b). We incorporated three different concentrations of GNPs (5, 10, and 20% v/v) into PEDOT: PSS. The current density–voltage (J–V) curves of the devices with the incorporation of GNPs under light conditions are shown in Fig. 3 (c). The performance parameters PCE, short-circuit current density (J_{SC}), open-circuit voltage (V_{OC}), fill factor (FF), series resistance (R_S), and shunt resistance (R_{SH}) for the control and various concentrations of GNP-incorporated NF-OSCs are shown in Fig. 3. For each condition, at least eight devices were fabricated to calculate average performance parameters. The PCE of the NF-OSCs initially increased and then decreased with an increase in the amount of GNPs in the HTL. Specifically, control solar cells without GNPs were obtained with an average efficiency value of 15.55%, resulting from a J_{SC} of 27.67 mA/cm^2, V_{CC} of 843 mV, and FF of 66.66%. After incorporating 5% v/v GNPs into the HTL, the best PCE of the champion solar cell enhanced was 16.55%, with an approximate enhancement of 6.43%. The PCE improvement is mainly due to the increase of J_{SC}, in which J_{SC} was improved from 27.67 mA/cm^2 to 28.60 mA/cm^2 in average. The trends in J_{SC} as a function of the GNPs concentration

are shown in Fig. 3 (b). Furthermore, the solar cells with 5% v/v GNPs showed a slight increase in V_{OC}, from 843 mV to 849 mV on average. However, a further increase in the concentration of GNPs to 10% v/v led to a decrease in the PCE of the solar cells to 15.42%, which resulted from a decrease in V_{CC} and FF. However, the average J_{SC} value remained invariant in comparison with solar cells with a GNPs concentration of 5% v/v. These results align with the observed increase in conductivity when GNPs were added to the HTL (Fig 2 (a)). This suggests that incorporating 5 and 10% v/v GNPs can achieve the most favorable conductivity for the hybrid HTL, potentially improving the hole transport in the devices. Consequently, this leads to an increase in the J_{SC}. On the other hand, the average PCE value for solar cells with a GNP concentration of 20% v/v decreased to 14.79%, which was mainly due to a decrease in V_{OC}. Notably, the average J_{SC} value for these solar cells remained above the J_{SC} value of the control cells.

As shown in Fig. 3 (e), the average R_S value of NF-OSCs with GNPs is higher than 1.70 Ωcm^2, comparing it with control solar cells, that is, NF-OSCs without CNPs, whose value is around 1.37 Ωcm^2. This shows that the R_S value increases with increasing GNPs concentration. A higher R_S value is a possible cause for the decreased FF value of the NF-OSCs with GNPs in the HTL. The R_{SH} also showed a definite trend; these values decreased with increasing concentrations of GNPs.

The improvement in performance owing to the increase in J_{SC} can be further demonstrated by the external quantum efficiency (EQE) spectra, as shown in Fig. 4 (a). The EQE spectrum of the solar cells with the incorporation of different amounts of GNPs into the PEDOT:PSS layer was enhanced in the wavelength region from 400 to 800 nm compared to the control device without GNPs addition. Solar cells with 5 and 10% v/v GNPs in the HTL exhibited the highest EQE intensity in the 350–800 nm wavelength range. The inset in Fig. 4 (a) shows the J_{SC} values obtained by integrating EQE with the reference spectrum AM 1.5G. These values corroborate the trend previously observed for J_{SC} regarding the GNPs concentration in NF-OSCs. The J_{SC} values obtained for the 5, 10, and 20% v/v were 28.46 mA/cm^2, 28.22 mA/cm^2, and 27.69 mA/cm^2, respectively. Therefore, the GNPs incorporated in the PEDOT:PSS can induce a pronounced EQE enhancement, which agrees well with the improvement in J_{SC} obtained from the J-V curves in Fig. 3 (c).

Additionally, to evaluate the charge recombination behavior of NF-OSCs, the relationship between V_{CC} and incident light intensity (LI) was studied under various intensities (from 10 to 100 mW/cm^2). Fig. 4 (b) shows V_{CC} as a function of the logarithm of *LI*. This dependency describes the order of the recombination process in the OSC and is commonly expressed as [23], [24]:

$$V_{OC} = n_{id}\left(\frac{kT}{q}\right)\ln(LI) + cte \tag{1}$$

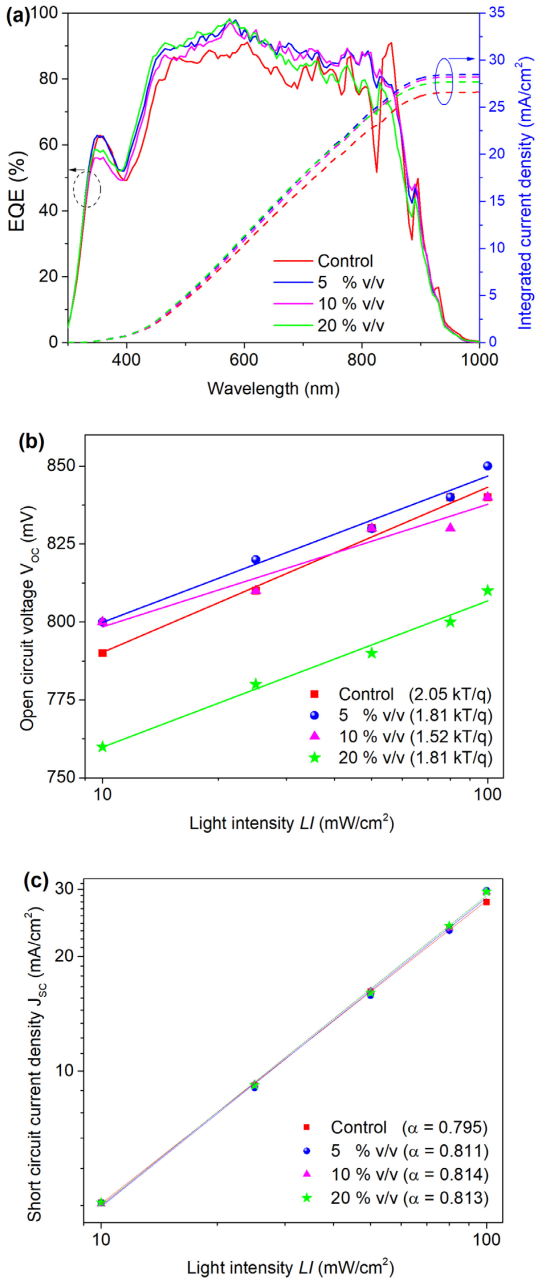

FIGURE 4. (a) EQE spectra of the devices with different GNPs amounts; light intensity dependence of (b) V_{CC} and (c) J_{SC} of the NF-OSCs with GNPs in the HTL.

where q, k, and T are the elementary charge, Boltzmann constant, and absolute temperature at 300 K, respectively, n_{id} is the ideality factor, and *cte* is an additional constant. It is well known that Langevin-type recombination is dominant when the slope of V_{CC} vs. ln (*LI*) approaches *kT/q* [24], [25]. However, a slope greater than *kT/q* is assumed for trap-assisted recombination, that is, a greater dependence on light intensity [25], [26]. As illustrated in Fig. 5 (b), the slopes of the solar cells with GNPs in the HTL show a slight decrease compared to those of the PEDOT:PSS solar cells. These values were 1.81, 1.52, and 1.81 for the 5, 10, and 20% v/v concentrations of GNPs, respectively. These observations

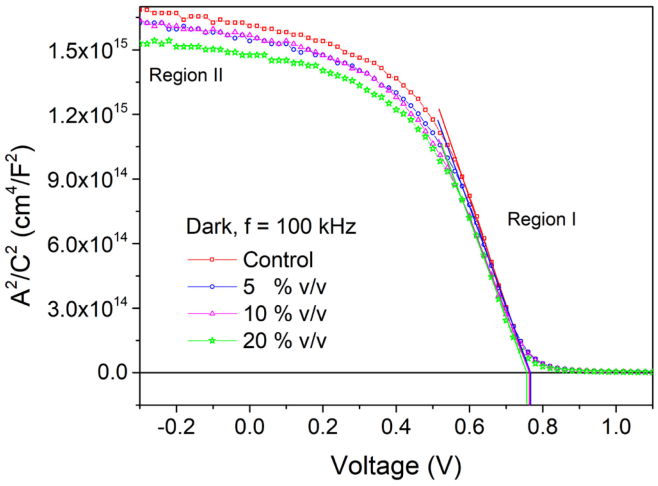

FIGURE 5. Mott Schottky curve under dark conditions at 100 kHz of different GNPs concentration of NF-OSCs.

indicate that Langevin-type recombination is not dominant in cells treated with GNPs or control cells. There is another type of recombination, called Shockley-Read-Hall (SRH), which involves trap-assisted recombination. The lower slope value for the solar cells with GNPs indicates that trap-assisted recombination was less dominant than that in the control cells. These results suggest that charge carriers in devices with GNPs have more time to contribute to the current generated by the cells. This, in turn, leads to an increase in the J_{SC}.

The relationship between J_{SC} and *LI* was further investigated to gain insights into bimolecular recombination in control and GNP solar cells. Fig. 4 (c) shows the plot of J_{SC} vs. *LI* on a log-log scale. J_{SC} can be related to *LI* using the power-law equations [4], [24], [27]:

$$J_{SC} \propto (LI)^{\alpha} \tag{2}$$

where *LI* is the intensity of the light and α is the exponential factor, which is obtained from the slope of the log-log scale plot of J_{SC} vs. *LI* [20]. If α is equal to 1 means in OSCs that the electrodes can effectively collect all free charge carriers before their recombination, implying that bimolecular recombination is insignificant [4], [24], [27]. The control solar cells exhibited a fitted exponential factor (α) of 0.795. In contrast, for the NF-OSCs with GNPs, the α values were 0.811, 0.814, and 0.813 for 5, 10, and 20% v/v, respectively. All the NF-OSCs with GNPs exhibited higher α values than the control solar cells, indicating that bimolecular recombination was less in the NF-OSC with GNPs than in the control solar cells. The decreased bimolecular recombination in the NF-OSC with GNPs can inhibit charge-carrier recombination and facilitate charge-carrier transport, which is conducive to a higher J_{SC} for the NF-OSC with GNPs in the HTL. The results demonstrated that the graphite nanoparticles improved solar cell performance.

In addition, capacitance-voltage (*C-V*) characteristics were applied to investigate the effect of GNPs addition in the HTL on the built-in potential (V_{bi}) of the NF-OSCs. Fig. 5 shows the Mott-Schottky curve of the *C-V* data obtained from measurements performed at a frequency of 100 kHz in the dark for NF-OSCs with different concentrations of GNPs into PEDOT:PSS. The curve for all cells exhibits two different regions: region I, at around 0.4 V to 0.8 V, corresponds to the contribution from the donor phase (PBDB-T-2F), while region II, which extends from −0.4 V to 0.4 V, have been attributed to the BTP-4CL acceptor phase [19], [28], [29]. The Mott-Schottky analysis was used to extract V_{bi} using the following equations [7], [28], [30]:

$$\frac{A^2}{C^2} = \frac{2}{q\varepsilon_0 \varepsilon N_A}(V_{bi} - V) \tag{3}$$

where *A* is the photoactive area of the cell, *C* is the capacitance, *V* is the applied voltage, *q* is the elementary charge, ε_0 is the vacuum permittivity, ε is the relative dielectric constant of the material, and *NA* is the charge carrier density. V_{bi} can be obtained from the intercept of the curve with the voltage axis. The obtained V_{bi} values were 0.767, 0.764, 0.757, and 0.763 V for the 5, 10, and 20% v/v concentrations of GNPs and the control, respectively. The V_{bi} value of solar cells with 5% v/v concentrations of GNPs in the HTL increased in comparison with the control. As the V_{bi} increases, a wider depletion region is formed, leading to improved separation of charge carriers and minimization of recombination losses [3], [31]. Consequently, the higher J_{SC} in the solar cells with 5% v/v concentrations of GNPs can be attributed to the higher V_{bi}. In addition, previous research has shown that incorporating graphite nanoparticles into the HTL improves the electrical conductivity of the layer [32], [33]. This can reduce the electrical resistance and enhance the hole transport efficiency, thereby increasing V_{bi}.

IV. CONCLUSION

We investigated the effects of incorporating different amounts of graphite nanoparticles (GNPs) into PEDOT:PSS as a hybrid hole-transport layer in non-fullerene organic solar cells. In this study, solar cells with the following structure were examined: ITO/HTL/PBDB-T-2F:BTP-4CL/PDINO/Ag. This study revealed a significant enhancement in the performance of the NF-OSCs with the addition of GNPs, particularly at a concentration of 5% v/v. The PCE of the NF-OSCs was enhanced to 16.55%, with a relative improvement of 6.43% compared to that of the control solar cells (15.55%). The addition of GNPs resulted in a remarkable improvement in the average PCE, which was primarily attributed to the increase in J_{SC}. This improvement in J_{SC} can be attributed to the improved light absorption, as evidenced by the enhanced external quantum efficiency (EQE) spectra. Moreover, analysis of the dependence of V_{CC} and J_{SC} on light intensity provided insight into

the contribution of recombination mechanisms. Bimolecular recombination was less significant in the NF-OSC with GNPs than in the control solar cells, indicating improved charge carrier collection efficiency. Furthermore, Mott-Schottky analysis through capacitance-voltage characteristics indicated that the addition of GNPs into the HTL increases the built-in potential (V_{bi}), promoting efficient charge carrier separation and reducing recombination losses. The combination of these improvements leads to an enhanced J_{SC}, consequently increasing the PCE of NF-OSCs with GNPs into the HTL with respect to those with only PEDOT:PSS as the HTL. This work demonstrates that the addition of GNPs into the HTL can effectively enhance the efficiency of OSCs and underscores the potential of these materials as promising materials for optimizing the performance of photovoltaic devices. Future research should focus on achieving even higher stability in NF-OSCs using GNPs.

REFERENCES

[1] T. Yu et al., "3D nanoscale morphology characterization of ternary organic solar cells," *Small Methods*, vol. 6, no. 1, Jan. 2022, Art. no. 2100916, doi: 10.1002/smtd.202100916.

[2] E. Moustafa, M. Méndez, J. G. Sánchez, J. Pallarès, E. Palomares, and L. F. Marsal, "Thermal activation of PEDOT:PSS/PM6:Y7 based films leads to unprecedent high short-circuit current density in nonfullerene organic photovoltaics," *Adv. Energy Mater.*, vol. 13, no. 4, Jan. 2023, doi: 10.1002/aenm.202203241.

[3] A. A. A. Torimtubun, M. Méndez, E. Moustafa, J. Pallarès, E. Palomares, and L. F. Marsal, "Achieving 17.7% efficiency of ternary organic solar cells by incorporating a high lowest unoccupied molecular orbital level and miscible third component," *Solar RRL*, vol. 7, no. 11, Jun. 2023, Art. no. 2300228, doi: 10.1002/solr.202300228.

[4] Y. Sun et al., "Rational control of sequential morphology evolution and vertical distribution toward 17.18% efficiency all-small-molecule organic solar cells," *Joule*, vol. 6, no. 12, pp. 2835–2848, Dec. 2022, doi: 10.1016/j.joule.2022.10.005.

[5] L.-K. Ma et al., "High-efficiency indoor organic photovoltaics with a band-aligned interlayer," *Joule*, vol. 4, no. 7, pp. 1486–1500, Jul. 2020, doi: 10.1016/j.joule.2020.05.010.

[6] J. Yuan et al., "Single-junction organic solar cell with over 15% efficiency using fused-ring acceptor with electron-deficient core," *Joule*, vol. 3, no. 4, pp. 1140–1151, 2019, doi: 10.1016/j.joule.2019.01.004.

[7] N. Tokmoldin et al., "Extraordinarily long diffusion length in PM6:Y6 organic solar cells," *J. Mater. Chem. A*, vol. 8, no. 16, pp. 7854–7860, 2020, doi: 10.1039/D0TA03016C.

[8] Y. Cui et al., "Organic photovoltaic cell with 17% efficiency and superior processability," *Nat. Sci. Rev.*, vol. 7, no. 7, pp. 1239–1246, Jul. 2020, doi: 10.1093/nsr/nwz200.

[9] D. Wang et al., "High-performance and eco-friendly semitransparent organic solar cells for greenhouse applications," *Joule*, vol. 5, no. 4, pp. 945–957, Apr. 2021, doi: 10.1016/j.joule.2021.02.010.

[10] H. Dahiya, R. Suthar, K. Khandelwal, S. Karak, and G. D. Sharma, "Recent advances in organic and inorganic hole and electron transport layers for organic solar cells: Basic concept and device performance," *ACS Appl. Electron. Mater.*, vol. 4, no. 11, pp. 5119–5143, Nov. 2022, doi: 10.1021/acsaelm.2c01076.

[11] C. Anrango-Camacho, K. Pavón-Ipiales, B. A. Frontana-Uribe, and A. Palma-Cando, "Recent advances in hole-transporting layers for organic solar cells," *Nanomaterials*, vol. 12, no. 3, p. 443, Jan. 2022, doi: 10.3390/nano12030443.

[12] Y. Lin et al., "17% Efficient organic solar cells based on liquid exfoliated WS_2 as a Replacement for PEDOT:PSS," *Adv. Mater.*, vol. 31, no. 46, Nov. 2019, doi: 10.1002/adma.201902965.

[13] J. Wang, H. Yu, C. Hou, and J. Zhang, "Solution-processable PEDOT:PSS:α-In_2 Se_3 with enhanced conductivity as a hole transport layer for high-performance polymer solar cells," *ACS Appl. Mater. Interfaces*, vol. 12, no. 23, pp. 26543–26554, Jun. 2020, doi: 10.1021/acsami.0c02489.

[14] D. Koo et al., "Improved charge transport via WSe_2 -mediated hole transporting layer toward efficient organic solar cells," *Semicond. Sci. Technol.*, vol. 33, no. 12, Dec. 2018, Art. no. 125020, doi: 10.1088/1361-6641/aaeab1.

[15] X. Zheng et al., "Solution-processed graphene-MoS_2 heterostructure for efficient hole extraction in organic solar cells," *Carbon*, vol. 142, pp. 156–163, Feb. 2019, doi: 10.1016/j.carbon.2018.10.038.

[16] J. Hao et al., "Broadband plasmon-enhanced polymer solar cells with power conversion efficiency of 9.26% using mixed Au nanoparticles," *Opt. Commun.*, vol. 362, pp. 50–58, Mar. 2016, doi: 10.1016/j.optcom.2015.07.032.

[17] J. Kastner et al., "Grinded nano-graphite inkjet inks for application in organic solar cells," *Nanotechnology*, vol. 30, no. 4, Jan. 2019, Art. no. 45601, doi: 10.1088/1361-6528/aae67a.

[18] A. Ali et al., "Super aligned carbon nanotubes for interfacial modification of hole transport layer in polymer solar cells," *Sustain. Mater. Technol.*, vol. 35, Apr. 2023, Art. no. e00569, doi: 10.1016/j.susmat.2023.e00569.

[19] E. Moustafa, J. Pallarès, and L. F. Marsal, "Investigating the role of PM6:Y7 layer thickness on optimizing non-fullerene organic solar cells performance through impedance spectroscopy analysis," *IEEE J. Electron Devices Soc.*, vol. 11, pp. 642–649, 2023, doi: 10.1109/JEDS.2023.3294888.

[20] M. Ramírez-Como et al., "Understanding the role of interfacial layers in the photostability of PM6:Y7-based organic solar cells under different degradation conditions," *Sustain. Energy Fuels*, vol. 7, no. 16, pp. 3883–3892, Jun. 2023, doi: 10.1039/D3SE00703K.

[21] C. K. Chua et al., "Synthesis of strongly fluorescent graphene quantum dots by cage-opening buckminsterfullerene," *ACS Nano*, vol. 9, no. 3, pp. 2548–2555, Mar. 2015, doi: 10.1021/nn505639q.

[22] B. Cui et al., "Fluorescent carbon quantum dots synthesized by chemical vapor deposition: An alternative candidate for electron acceptor in polymer solar cells," *Opt. Mater.*, vol. 75, pp. 166–173, Jan. 2018, doi: 10.1016/j.optmat.2017.10.010.

[23] M. Ramirez-Como et al., "Solution-processed small molecule inverted solar cells: Impact of electron transport layers," *IEEE J. Electron Devices Soc.*, vol. 10, pp. 435–442, 2022, doi: 10.1109/JEDS.2022.3165315.

[24] S. R. Cowan, A. Roy, and A. J. Heeger, "Recombination in polymer-fullerene bulk heterojunction solar cells," *Phys. Rev. B, Condens. Matter*, vol. 82, no. 24, Dec. 2010, Art. no. 245207, doi: 10.1103/PhysRevB.82.245207.

[25] S. R. Cowan, W. L. Leong, N. Banerji, G. Dennler, and A. J. Heeger, "Identifying a threshold impurity level for organic solar cells: Enhanced first-order recombination via well-defined $PC_{84}BM$ traps in organic bulk heterojunction solar cells," *Adv. Funct. Mater.*, vol. 21, no. 16, pp. 3083–3092, Aug. 2011, doi: 10.1002/adfm.201100514.

[26] B. Liu et al., "Boosting efficiency and stability of organic solar cells using ultralow-cost BiOCl nanoplates as hole transporting layers," *ACS Appl. Mater. Interfaces*, vol. 11, no. 36, pp. 33505–33514, Sep. 2019, doi: 10.1021/acsami.9b12583.

[27] P. Hartnagel and T. Kirchartz, "Understanding the light-intensity dependence of the short-circuit current of organic solar cells," *Adv. Theory Simul.*, vol. 3, no. 10, Oct. 2020, Art. no. 2000116, doi: 10.1002/adts.202000116.

[28] B. Ecker et al., "Degradation effects related to the hole transport layer in organic solar cells," *Adv. Funct. Mater.*, vol. 21, no. 14, pp. 2705–2711, Jul. 2011, doi: 10.1002/adfm.201100429.

[29] J. C. Nolasco et al., "Relation between the barrier interface and the built-in potential in pentacene/C_{60} solar cell," *Appl. Phys. Lett.*, vol. 97, no. 1, Jul. 2010, Art. no. 13305, doi: 10.1063/1.3456393.

[30] A. S. Grove, *Physics and Technology of Semiconductor Devices*. Hoboken, NJ, USA: Wiley, 1967, doi: 10.1016/0016-0032(69)90128-8.

[31] Y. Zhu, T. Song, F. Zhang, S.-T. Lee, and B. Sun, "Efficient organic-inorganic hybrid Schottky solar cell: The role of built-in potential," *Appl. Phys. Lett.*, vol. 102, no. 11, Mar. 2013, Art. no. 11350, doi: 10.1063/1.4796112.

[32] Z. Xia et al., "Two-dimensional graphitic carbon nitride for improving the performance of organic solar cells," *J. Phys. Chem. Lett.*, vol. 14, no. 29, pp. 6532–6541, Jul. 2023, doi: 10.1021/acs.jpclett.3c01536.

[33] X. Li et al., "Amine-functionalized carbon dots as PEDOT:PSS dopants for organic solar cells," *Adv. Mater. Interfaces*, vol. 10, no. 35, Dec. 2023, Art. no. 2300502, doi: 10.1002/admi.202300502.